Chapter 2

Materials Preparation and Characterisations

2.1 Materials Preparation and Characterisations

There are several techniques for the synthesis of ceramic oxides [166]. Each approach has pros and cons. The preparative approach was chosen in accordance with the experimental resources available at the department's research lab. In the current work, solid state ceramic approach, a straight forward technique, is used to synthesize to synthesize undoped and La, Sn, Nb doped Sr_2SnO_4. It is a common mechanical alloying technique that is used to create different kinds of ceramic oxides.

Each compound needs to be characterised after its synthesis in order to understand its structural and physical property, as well as potential uses or applications. The characterisation of material plays vital role in understanding the fundamental Physics involved in it. Henceforth, in this thesis work a standard protocol is followed for synthesis and characterisation of materials. The undoped and doped compositions of Sr_2SnO_4 are synthesized using conventional solid state ceramic route, at first, thereafter each synthesized composition were characterized using modern and advanced sophisticated instruments. The structural characterisations were done using X-ray diffraction (XRD) technique using X-ray Diffractometer, followed by Rietveld refinement of X-ray diffraction pattern. To investigate the morphology and microstructure of synthesized compositions Field emission scanning electron microscopy (FESEM) technique is used. The presence of the rotational, vibrational band, and other functional groups was investigated using Fourier transform infrared (FTIR) spectroscopy. A UV-Vis-NIR spectrometer is used to investigate the prepared compositions' absorption, and a well-defined Tauc's relation is used to determine the optical band gap. The X-Ray Photoelectron Spectroscopy (XPS) technique is used to study the valence state of doped element as well as parent elements in undoped and doped Sr_2SnO_4. At last, the electrical and dielectric properties of the synthesized undoped and doped Sr_2SnO_4 compositions were studied. The frequency and

temperature dependent impedance of synthesized compositions is measured using high precision LCR meter operating between 20 Hz to 2 MHz while heating the samples at different temperatures from 30 ^{o}C to 600^{o}C. The electrical and dielectric parameters is calculated from the measured impedance data and analysed.

The physics of the synthesis method and the experimental techniques employed & the fundamental principles of employed instruments in the study are summarized and articulated subsequently in this chapter.

2.2 Materials Synthesis

The synthesis of material via conventional solid state ceramic route involves following steps:

2.2.1 Selection of raw materials

Undoped Sr_2SnO_4 and La, Sn and Nb doped samples have been prepared by conventional solid state ceramic route by ball milling process in present thesis work. The raw precursors taken for sample preparation is tabulate in Table .2.1 The schematic representation of the methodology followed for sample preparation is shown in Fig. 2.2.

Table 2.1 Specification of materials used in synthesis.

Raw Materials	**Purity (%)**	**Manufacturer**
$SrCO_3$	≥ 99.9	Sigma-Aldrich
MnO_2	≥ 99	Sigma-Aldrich
La_2O_3	≥ 99.9	Alfa Aesar
SnO_2	≥ 99.9	Alfa Aesar
Nb_2O_5	≥ 99.9	Alfa Aesar

2.2.2 Weighing of raw materials

The accurate weighing of raw materials in the stoichiometric amount is perhaps the most important unit of operation involved in materials synthesis, since no amount of mechanical processing can make up for any deficiencies in raw materials which have been omitted from the mixture. The point at which weighing occurs in the synthesis process depends upon the design of the mill. Raw materials may be selected, weighed and then subjected to grinding and mixing, or materials may be pre-ground, then weighed and mixed. There are advantages and disadvantages in both approaches and their choice depends upon the raw materials to be processed and the design considerations of machinery manufacturers. In current thesis work, since raw materials required for sample preparation is small. Thereby, the raw materials were weighed individually on a platform of digital weighing machine, then mixed using of ball mill.

2.2.3 Mixing of raw materials using ball mill

2.2.3.1 Mechanical Milling or Alloying

The first mechanical alloying procedure for sample preparation that was both affordable and time-efficient was created by Benjamin, his co-workers, and their International Nickel corporation in the late 1960s. In the late 1900s, researchers started to adopt this technology more when it comes to synthesize novel phases and structures of oxide materials. The energy is produced in this process by the ball's rapid spin inside the pot. This method, also known as high energy ball milling, is commonly used to prepare nanomaterial of different ceramic oxides. From the commercially accessible basic ingredients, the mixture of the desired compositions can be synthesized. By activating and calcining the starting material, new compounds, new structures, and new phases can be synthesized under control atmosphere.

In this procedure, the powder precursors are kept inside the tightly closed vial with small spherical balls, which is made of the same material as the vial. The vials are rotated for a

specific amount of time at a predetermined rotation speed. While high energy ball milling of precursors power, the powder experiences various processes like fracturing, welding, griding to nanoscale dimensions, homogenous mixing, etc., thereby the formation of new phases and compounds is initiated. In order to prevent chemical reactions between the precursors and the vial and balls, the selectivity of the vial and ball material was dependent on the type of chemical utilised in sample preparation. In general, Vials and balls are typically made of stainless steel, Zirconia Dioxide, Tungsten Carbide, etc.

2.2.3.2 Mechanism of Ball-Mill

The mechanism of a planetary ball mill is shown in Fig. 2.1. The grinding action depends upon velocity and force of the balls colliding with the sample, solely dependent on the rotation speed of disc (Ω), the rotational speed of the vials around the disc (ω), the radius of the disc (R) and the vials (r), the mass or weight of the ball (m), and the number of balls (n). In a planetary ball mill, the power of the shock and the energy supplied to the powder during each collision with the ball minimally affect the formation of the final products. The mathematical formula power (P) of the shock is:

$$P \propto ml^2\Omega^2\omega \qquad (2.1)$$

Where, l^2 is the characteristic area.

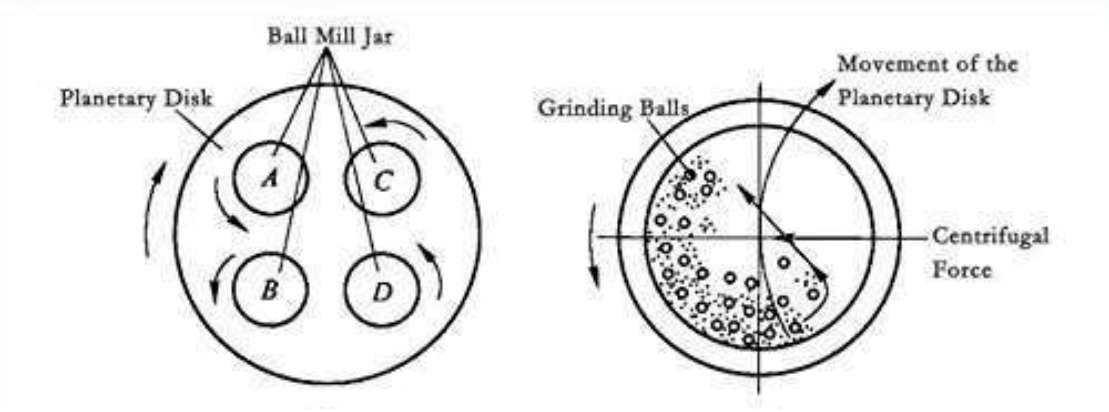

Figure 2.1. Working Principle of Lab Planetary Ball-Miller.

Through a series of processes, the shock energy produced between collisions of the balls with the inner wall of the closed vial transforms the precursor of raw materials into the fine powder. The powder is first blended during the mixing process, then it fragments, then it coalesces, and finally it goes through phase transformation and amorphization. The milling circumstances, including the milling atmosphere, the beginning powder composition, the mass ratio of the balls to the powder, the materials used to make the balls and vials, the typical milling time, and the temperature produced by the milling process, all affect the final product's nature. There are certain advantages and disadvantages of Ball Milling process(es), listed below.

Advantages

I. Low-cost installation and grinding medium.

II. One pot, one step mechano-synthesis.

III. Fabrication of materials at room temperature.

IV. Revolution per minute (rpm) and milling time can be programmed for user-defined.

V. Suitability of choosing milling atmosphere.

VI. Applicable to materials having all degree of hardness.

VII. Synthesis of a new phase is possible with localized deformation.

VIII. Formation of particles in the nano dimension or even in the amorphous phase and also controls the particle size of final product.

IX. Formation of a complete solid solution.

X. Complex powder formation in a concise time.

XI. Various milling parameters can control shock energy.

Disadvantages

I. Contamination from the milling medium.

II. Stickiness of the sample with container results loss of materials.

III. Excessive heating during milling.

By addressing the drawbacks listed above, milling parameter can be optimized. To prevent contamination from the milling media, the milling period must be adjusted over time and from sample to sample. Controlling the vials' speed will reduce the extra heat produced during milling. To ensure the purity of the finished product, the balls to powder mass ratio (BPMR) and milling environment are adopted.

2.2.3.3 Preparation of mixture of raw materials using Ball Milling

In the current thesis, for preparation of specified compositions (in Table 1.2), a vial made up of chrome steel (the inside layer of which is covered with Agate) and five Agate balls, each measuring 10 mm in diameter are taken. A 100 ml chrome steel vial with stoichiometric amounts of the basic components listed in Table 2.1 is partially filled with Agate balls (1:40 balls to mass ratio). The closed steel vial is then mounted to a planetary ball mill (PM 200, Retsch, Germany) and revolved for 8 hours while pausing occasionally at a speed of 200 rpm. Due to the centrifugal force between the balls and inner wall, the high-speed rotation of vial produces a collision between the balls and sample. For uniformly grinding of the samples, balls are kept inside the vials with the samples. The milled powder is then transferred from the vial to a Platinum crucible and dried in an oven for 24 hours at 60 ^{o}C. Dried powders were then transferred to an agate mortar and grounded one more time to ensure homogeneity of precursor's mixture.

2.2.4 Calcination of Mixtures

Calcination is the process of heating a solid to a high temperature below its melting point in order to produce a condition for thermal decomposition or a phase transition other than melting or fusion. To produce single phase powder, the resultant mixture was transferred to a Platinum crucible and placed inside the programmed muffle furnace. The calcination temperature, time

and other parameters are specific to the prepared compositions mentioned in their succeeding chapters. To follow successful preparation of the intended compositions, their samples were put through a number of different characterization approaches, some of which are covered in the succeeding sections.

2.2.5 Granulation or Palettization

After calcination, the powder was uniformly grinded in an agate mortar with a pestle. For pelletization, 2% Polyvinyl Alcohol (PVA) was uniformly blended and grinded it into the powder until it was very fine. The final step was to pelletize the fine powder using a hydraulic press and a die with a 10 mm diameter under 5 kN of pressure. The pellets that have been obtained are then anticipated for additional characterisation.

2.2.6 Sintering of Pellets

Figure 2.2. Flowchart of materials preparation.

Sintering is the heating technique used to modify the material's microstructure, make it denser, and promote crystal growth. The materials were sintered during the course of multiple thermal heating stages. In order to completely burn off the binder, the furnace was heated to

200 °C at a heating rate of 2°C/min for 2h. Then, pellets were heated to 1500°C at and maintained there for 12 hours to begin the sintering process. The pellets were then cooled to room temperature with different cooling rates.

The next section describes the additional characterization techniques that were used to investigate the phase development, microstructure, electrical and dielectric characteristics of prepared compositions(pellets)

2.3 Characterization

2.3.1 X-ray diffraction analysis

2.3.1.1 Methodology

Powder X-ray diffraction is a vital characterisation method for phase identification in the field of material science that has been developed over time. The powder X-ray diffraction is an experimental technique that links the XRD pattern from crystal structure of packed powder specimen. The wavelength of X-ray is of the order of atomic spacing in crystal structure. Hence the 3D atomic arrangement of crystal acts as a grid for X-rays. When culminated X-rays shined on the crystal, a diffraction pattern is generated. Physically when X-rays are shined, the electrons in the crystal starts oscillating with the x-ray's frequency, generates secondary X-rays and radiates it in all 3D directions. When these scattered secondary X-rays interfere constructively, generates diffraction peaks in a certain direction, which contains the signature of atomic arrangement in crystal. In simplified terms, it is understandable that the formation of the XRD pattern was caused by the X-ray diffraction from countless tiny polycrystals in the powder samples that were randomly oriented domains in all directions. The group of domains in randomly oriented domains diffracting X-rays in one common direction are classed as coherently diffracting domains. The X-ray diffraction method is a most powerful and widely used technique for studying crystal structure and lattice spacing. It can also be used

for phase identification, calculating crystallite size, stress measurement and for analysing crystals with one preferred crystallites orientation in polycrystalline aggregate [167]. It is a non-destructive experimental analysing technique, and samples can be exposed to various pressure and temperature conditions while the diffraction pattern is being collected.

In 1913, English physicists Sir W.H. Bragg and Sir W.L. Bragg developed a relationship to explain why the cleavage faces of crystals appear to reflect x-ray beams at certain angles of incidence .The relation is known as Bragg's law, given as follows:[168]

$$2d_{hkl}\sin\theta = n\lambda \qquad (2.2)$$

where, d_{hkl} is the interplanar spacing of (hkl) sets of planes, λ is x-ray wavelength, θ is angle of incident X-ray from exposed crystal face, and, n is an integer and said to be an order of diffraction.

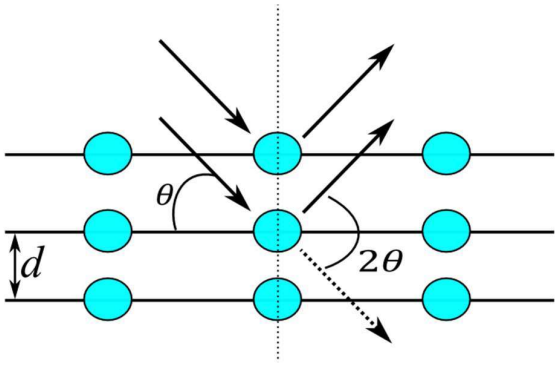

Figure 2.3. Schematic illustration of X-ray diffraction from a crystal.

The Bragg's law can be obtained geometrically, as depicted in Fig. 2.4.

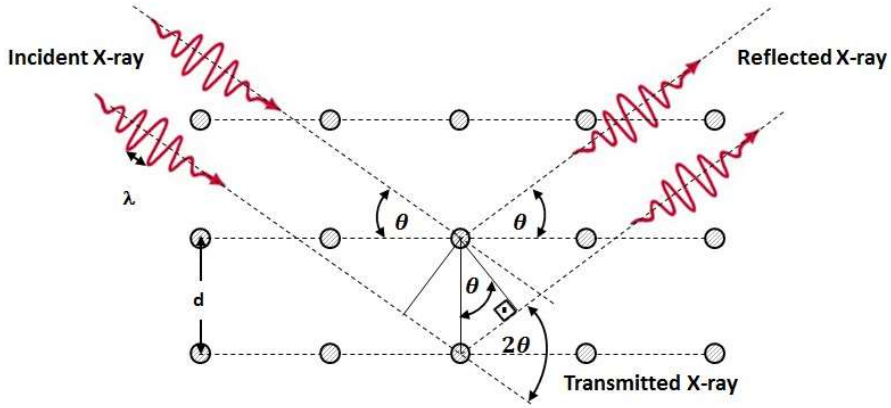

Figure 2.4. Visualization of Bragg's law.

Let us consider a set of crystallographic lattice planes with an interplanar spacing d_{hkl} is irradiated by X-ray waves. Let θ be the angle of incidence between X-ray beam and lattice plane, the interplanar spacing d_{hkl} creates a path difference for the ray scattered from two consecutive the atomic planes. Using geometry, the path difference between incident and diffracted ray can be calculated to be $2d_{hkl}\sin\theta$. If the path difference is an integral multiple of wavelength (λ), then the interference between the scattered rays can be said to be constructive. There by the Bragg's law mathematically can be written as:

$$2d_{hkl}\sin\theta = n\lambda \qquad (2.2)$$

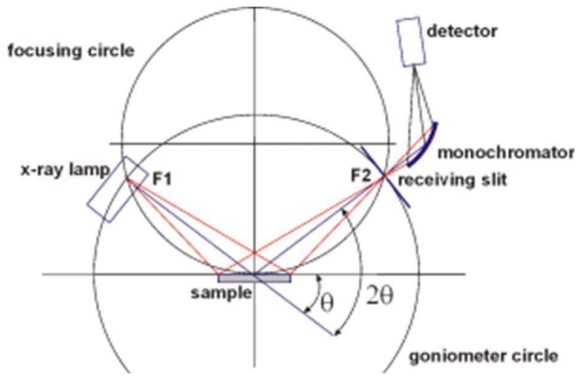

Figure 2.5. Schematic representation of θ/2θ diffraction in Bragg-Brentano geometry.

Fig. 2.5 depicts the fundamental geometry that the majority of X-ray diffractometers use. The incident and scattered rays' angles with respect to the specimen surface is θ. By

changing the scattering angle by 2θ and the incidence angle of the X-ray beam by θ angle, the XRD pattern is recorded. The scattering intensity (I) generally reported as a function of 2θ. In some instances, the sample is rotated by angle θ and the detector is moved by 2θ while the X-ray source remains fixed. In most of the diffractometer, the sample is kept stationary while the X-ray source and detector are both simultaneously rotated by θ angle. The goniometer, which is the instrument's core component, rotates source and detector with such accuracy. Typically, the X-ray source and detector move around the periphery while the sample is positioned on the rotational axis.

2.3.1.2 Phase Matching

The peaks in the powder XRD pattern are produced by randomly oriented planes are identified by the corresponding Miller indices (hkl). The conventional phase identification approach is used to index and match the peaks in the recorded XRD pattern. The Miller indices, relative intensities, similar interplanar spacings or diffraction angles, and other crystallographic data are used in the standard phase identification approach [169]. The "**International Center for Diffraction Data (ICDD)**" formerly the "**Joint Committee for Powder Diffraction Standards (JCPDS)**" maintains the standard database. Another free database called "**Crystallographic Open Database (COD)**" is accessible to users. The experimental XRD pattern is matched with the COD database in the current thesis work. The simulation approach, which is an additional alternative to the search match method, uses structural data from the ICDD database to enable a computer programme to produce the theoretical XRD pattern. This method is only applicable when the crystal phase(s) or similar structure file is available in the ICDD database. By adjusting a number of instrumental, structural, and microstructural factors throughout the continuous iteration process, the gross computed XRD pattern is then refined to better fit the experimental XRD pattern [170].

2.3.1.3 Rietveld Refinement Analysis

The Rietveld method is proposed in International Union of Crystallography (IUC) stated as "**Method of analysing powder diffraction data in which the crystal structure is defined by fitting the entire profile of the diffraction pattern to a calculated profile using a least-square approach. There is no intermediate step of extracting structure factors, and so patterns containing many overlapping Bragg peaks can be analysed**" [170]. That is The Rietveld Refinement analysis is used to analyse the crystallographic information like, phase, space group, lattice parameters, crystallographic angles, strain in the structure, etc. For this purpose, the peak position available in the experimentally recorded XRD pattern is matched with the available crystallographic information in the Crystallographic Open Database (COD) for different crystallographic phase(s) of the material. After phase identification, individual detailed structure file so-called crystallographic information file (CIF) is taken as preliminary information for further processing of experimentally recorded XRD pattern. The Rietveld refinement software simulates a theoretical XRD pattern from the input CIF file. Apart from this preliminary information some other information is also required for structural and microstructural characterizations like, (i) instrumental correction factors, such as peak shift, peak broadening, and peak asymmetry; and (ii) an approximation of crystallite size and lattice strain.

To get the structural and microstructural characteristics, the simulated XRD pattern iteratively refines the experimental XRD pattern while holding a different parameter constant. In this instance, the Marquardt least squares fitting approach has been applied. By gradually improving structural and microstructural parameters until they converge, the "best fit" between the intensities of the simulated and experimental XRD patterns is obtained. Through the least square method, the amount S_y is minimised, defined as follows:

$$S_y = \sum_i W_i(I_{oi} - I_{ci})^2 \qquad (2.3)$$

Here, $W_i = 1/I_{oi}$, I_{oi} = observed intensity at i^{th} step and I_{ci} =calculated intensity at i^{th} step. The best fit is achieved when S_y attains a minimum value. The value of I_{ci} is obtained by summation of all calculated intensities and background contribution given by;

$$I_{ci} = S\sum_k L_k|F_k|^2 \emptyset(2\theta_i - 2\theta_k)P_k A + I_{bi} \qquad (2.4)$$

Here, S is the scale factor, L_k contains Lorentz polarization factor and multiplicative factor, k represents Miller indices hkl for a Bragg reflection, F_k is the structure for k^{th} Bragg reflection, $\emptyset$ is a reflection profile function which approximate the effect of aberration due to absorption, specimen displacement, crystallite size, microstrain etc., P_k is the preferred orientation function, A is an absorption factor, I_{bi} is the background intensity of i^{th} step, $2\theta_k$ is the diffraction angle of k^{th} Bragg reflection.

Due to the inclusion of numerous parameters, the Rietveld refining of the X-ray diffraction pattern is a crucial procedure. To accomplish that, sophisticated software that may easily be used is needed to correlate the calculated and experimental XRD patterns at each stage. Many people throughout the world uses free Rietveld software, including the FullProf software package, which was employed in the current thesis work for Rietveld refinement study.

The X-ray powder diffraction data generated by H.M. Rietveld in 1969 are refined using Rietveld software [171]. Without knowing the crystal structure, this software programme is also utilised as a profile matching tool. With the incorporation of all recent developments, this programme is capable of analysing the numerous structural and microstructural aspects. Fig. 2.6 depicts a typical FullProf software interface. This programme is used to examine X-ray diffraction patterns from bulk to nanoscale materials.

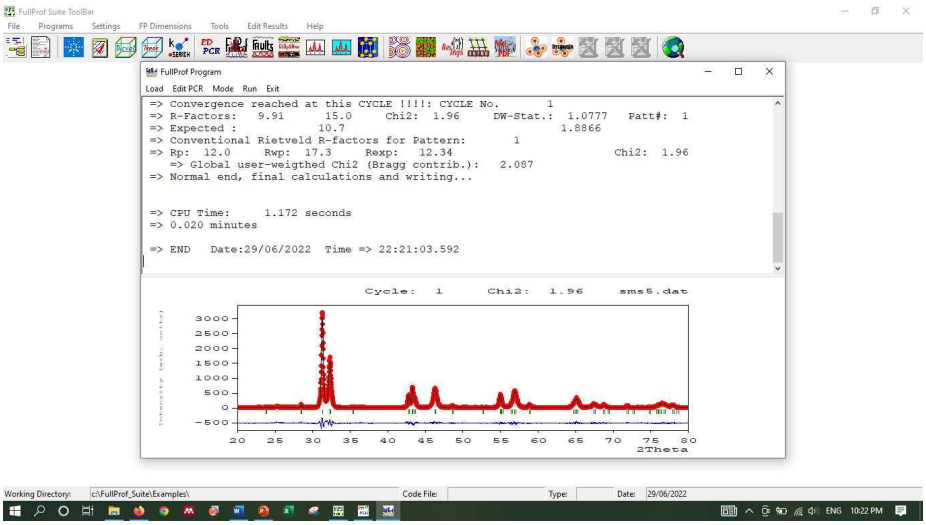

Figure 2.6. A typical FullProf software interface during Rietveld refinement process.

There are certain features and advantages of FullProf software package, are follows:

1. This programme can be used to refine the X-ray diffraction data obtained from neutron and synchrotron sources as well as laboratory setup sources.
2. Various functions, such as constant functions and higher order polynomials through Fourier filtering, can be used to generate the backgrounds data.
3. For each phase, the peak shape is represented using a number of functions, including split pseudo-Voigt, Pearson-VII, Thompson-Cox-Hashing (TCH) pseudo-Voigt, and the convolution of a double exponential with a TCH pseudo-Voigt.
4. Multiple phases can be refined using the Rietveld method (upto 16 phases).
5. For modelling the preferred orientation of a peak, two different types of functions are offered.
6. There are micro-absorption corrections for the Bragg-Brentano setup as well as absorption corrections for various geometries.
7. It provides the choice of automatic generation of hkl and/or symmetry operators.
8. It is also possible to refine magnetic structures.

9. Automatic generation of reflections for an incommensurate structure upto 24 propagation vectors.
10. hkl dependence of the position shifts of Bragg reflections for special kind of defects.
11. Quantitative analysis has been performed without the need for structure factor calculations.
12. The instrumental resolution function (Voigt function) may be supplied in a file then the microstructural analysis is then performed.
13. Popa-Balzer model can add anisotropic crystallite size and strain.
14. For a better view of the simulated pattern along with the experimental pattern, the square root of intensity is plotted against 2θ.

The scale factor of Rietveld refinement directly affects the quantitative measurement of various phases that are present in a multiphase complex [172]. For a multiphase system with known molecular weight, the weight fraction phase can be calculated using the relation;

$$W_i = \frac{S_i(ZMV)_i}{\sum_j S_j(ZMV)_j} \qquad (2.5)$$

Here, S_i is the scale factor, Z_i is the number of molecules per unit cell, M_i is the molecular weight and V_i is the unit cell volume of i^{th} phase present. The density of i^{th} phase can be evaluated using the following relation-

$$\rho_i = \frac{Z_i M_i}{N_A V_i} \qquad (2.6)$$

N_A is Avagadro number. In multiphase compound(s), for various scientific and industrial applications, it is crucial to calculate the relative phase abundances. It was discovered that the Rietveld analysis was a very effective way for figuring out the phase fraction of multiphase materials.

Various structural and microstructural parameters is minimized by irritative approach in the Rietveld refinement for fitting X-ray diffraction profiles [170]. These techniques alter various parameters until the difference between experimental intensities (I_{oi}) and calculated intensities (I_{ci}) is as small as possible. The quality of fitting is determined by the residue parameters listed below.

The residue of structure factor,

$$R_F = \frac{\sum_i \left|\sqrt{I_{oi}} - \sqrt{I_{ci}}\right|}{\sum_i \left|\sqrt{I_{oi}}\right|} \qquad (2.7)$$

The residue of Bragg factor,

$$R_B = \frac{\sum_i |I_{oi} - I_{ci}|}{\sum_i |I_{oi}|} \qquad (2.8)$$

The residue of weighted pattern,

$$R_{wp} = \left|\frac{\sum_i W_i (I_{oi} - I_{ci})^2}{\sum_i W_i (I_{oi})^2}\right|^{1/2} \qquad (2.9)$$

The residue of expected pattern,

$$R_{exp} = \left|\frac{N - P}{\sum_i W_i (I_{oi})^2}\right| \qquad (2.10)$$

In all the equation I_i is the intensity of i^{th} Bragg reflection at the end of the refinement, the letter o and i in suffix represents the observed and calculated intensities. W_i and N represents the weight and number of experimental observation and P represents the number of refineable parameters. The refinement process has been continued till convergence of this parameter is reached. The quality of fit is also monitored by "Goodness of fit" (GoF) defined as

$$\mathrm{GoF} = \frac{R_{wp}}{R_{exp}} \qquad (2.11)$$

For best fit, the GoF is approx. 1.00, which means, the calculate pattern fully matched with the experimental pattern.

On highly resolvable diffraction data, the Rietveld refinement analysis of the powder XRD pattern from a polycrystalline sample was carried out. The XRD data were captured for this use in step scan mode with a slow scanning rate. With the help of an X-ray diffractometer (Rigaku Miniflex II, Japan) and Cu K radiation with a wavelength of 1.5418 at an applied voltage of 40 kV and current of 40 mA, the various crystallographic phases of the present sample were collected. With a step size of 0.02° and a scan rate of 0.02° degree per minute, the XRD pattern has been recorded in the angular range of 20° to 80°. For X-ray diffraction studies, we employed main divergence slits that were 0.6 mm wide and secondary divergence slits that were 1.0 mm wide. Fig. 2.7 depicts the X-ray diffractometer used for the current thesis project.

Figure 2.7. X-ray diffractometer (XRD) at Central Instrument Facility (CIF) IIT (BHU).

2.3.1.4 Size-Strain Analysis

The Size-Strain plot (SSP) method has been used to analyse the XRD pattern in order to study the microstructural examination of a polycrystalline compound in terms of crystallite (particle) size, lattice strain, and flaws (dislocations and stacking faults). Practically speaking, no

polycrystalline sample is perfect in the sense that the diffraction peaks are widened with finite peak widths. The broadening in XRD peaks is appeared due to (i) Instrumental broadening (ii) Small crystallite size (iii) Accumulation of lattice strain (iv) Presence of different kinds of stacking faults in the lattice.

The examination of the diffraction pattern using the integral breadth method can forecast the composition's microstructure and finite particle size. This approach was first proposed by Scherer in 1918 [167], and it was later improved upon by Stokes and Wilson [173]. This is the most traditional technique used for determining particle size and strain. According to this method, the angular width of the peak in radians at the location where the intensity drops to half its greatest value, i.e., full width at half maxima (FWHM) is used to define the breadth of the diffraction line. Max-Von Laue also suggested the following approach for calculating the breadth of the diffraction peak.

$$\beta = \frac{1}{I_p}\int I(2\theta)d(2\theta) \qquad (2.12)$$

Here, β is "integral width", I_p is the peak intensity and $I(2\theta)$ is intensity at diffraction angle 2θ. In 1949, Hall proposed that the integral width should be defined as the sum of two broadenings given by (After correction of instrumental broadening and neglecting broadening due to lattice imperfections):

$$\beta = \beta_D + \beta_S \qquad (2.13)$$

Here, β_D and β_S are peak broadening due to small crystallite size and microstrain in lattice respectively. The β_D is measured by Scherrer equation-

$$\beta_D = \frac{k\lambda}{D\text{Cos}\theta} \qquad (2.14)$$

Where, λ is X-ray wavelength, k is the crystallite shape constant (k = 0.89 for spherical shape), D is the crystallite size, and θ is the Bragg angle. β_S is the broadening arising from the microstrain in the compound given by:

$$\beta_S = 4\epsilon \tan\theta \qquad (2.15)$$

Where, ϵ is the microstrain in the lattice, so Eqn. (2.14) can be rewritten as;

$$\beta = \beta_D + \beta_S = \frac{k\lambda}{D\cos\theta} + 4\epsilon \tan\theta \qquad (2.16)$$

$$\frac{\beta\cos\theta}{\lambda} = \frac{1}{D} + \frac{4\epsilon\sin\theta}{\lambda} \qquad (2.17)$$

Thus, by measuring the FWHM (β) and corresponding Bragg angle of all reflection appeared in the XRD pattern of the polycrystalline sample. A straight line (best fit) using Eqn. (2.17) obtained by plotting the curve between $\frac{\beta\cos\theta}{\lambda}$ along ordinate and $\frac{\sin\theta}{\lambda}$ along abscissa is known as Williamson-Hall Plot. The intercept of the straight line on ordinate gives the measure of $\frac{1}{D}$ and slope of the straight line gives the measure of average microstrain (ϵ).

The line broadening in XRD peaks is largely thought to be isotropic in the Williamson-Hall plot. This suggests that microstrain contribution was also present and the diffracting domains were isotropic. However, the "Size-Strain plot (SSP)" method produced a better evaluation of the size-strain parameters in the situation of isotropic line broadening. The benefit of this strategy is that data gathered at high angles, when prerecession is often lower, have been given less weight. In this approximation, the crystallite size profile is considered to be a Lorentzian function and the strain profile by a Gaussian function [134,139]. Accordingly, we have

$$\left(\frac{d_{hkl}\beta\cos\theta}{\lambda}\right)^2 = \frac{k\lambda}{D}\left(\frac{{d_{hkl}}^2\beta\cos\theta}{\lambda^2}\right) + \left(\frac{\varepsilon}{2}\right)^2 \qquad (2.18)$$

Where d_{hkl} is the interplanar spacing corresponding to the plane (hkl), ε is the average strain produced in the lattice, k is a constant which depends on the shape of particles, for example, it is ¾ for a spherical particle. Similar to the W-H plot, the term $\left(\frac{d_{hkl}\beta\cos\theta}{\lambda}\right)^2$ is plotted with respect to $\left(\frac{{d_{hkl}}^2\beta\cos\theta}{\lambda^2}\right)$ for all diffraction peaks. The particle size was determined from the slope of the linearly fitted data while the square root of the intercept gives the strain.

2.3.2 Field Emission Scanning Electron Microscope (FESEM)

The field emission scanning electron microscope (FESEM) can be used to observe features on the surface of materials that are as small as 1 nm. According to the needs, the observation's magnification can be changed and taken into account. Organelles and nuclei of cells, synthetic polymers, and coatings are a few examples of things that can be studied with a FESEM in practise. It is also appropriate for describing the morphology and geometry of electrospun nanofibers.

Fig. 2.8 shows a typical Field Emission Scanning Electron Microscope (FESEM). FESEM uses electrons with a negative charge in place of light. A field emission cathode in electron gun of a scanning electron microscope provides a narrower beams at low as well as high electron energy, resulting in both improved spatial resolution and minimized sample charging and damage [174]. Field emission electrons are then accelerated in a strong electrical field gradient. These so-called primary electrons are focussed and refracted by electronic lenses within the high vacuum column to create a narrow scan beam that bombards the target. The electron beam stimulates emission of high-energy backscattered electrons and low-energy secondary electrons from the surface of the specimen. These secondary electrons' angles and velocities are related to the object's surface structure. The specimen surface is scanned by moving electron gun over it in zigzag manner. The secondary electrons emitted from every spot of specimen

surface are captured by a detector, which then converted in the form of an electrical signal. This signal is amplified and transformed to a monitor or to a digital image that can be saved and processed. The FESEM produce a clear, less electrostatically distorted image of specimen with spatial resolution to 50 nm, which is 10 to 100 times better than conventional SEM.

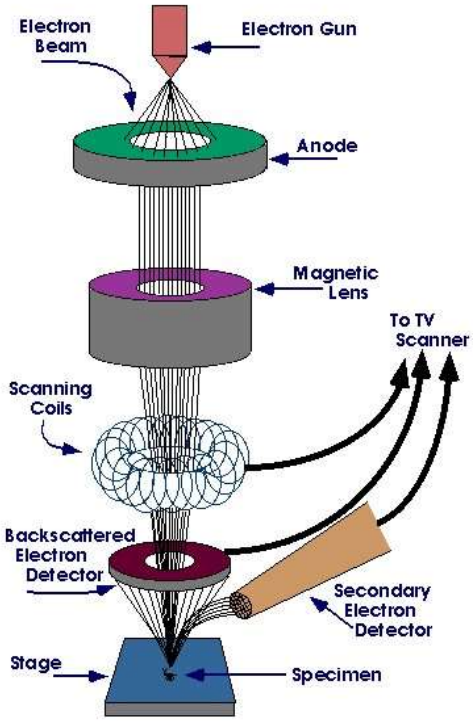

Figure 2.8. The Schematic view of a Field Emission Scanning Electron Microscope (FESEM).

The FESEM looks like a desk-mounted cylindrical column. The electron beam is housed in the column. At various heights of the column, there are knobs for controlling the electron beam. The SEM does not require complex specimen preparation procedures, large and bulky specimens can be examined. In order to obtain a clear image, it is preferable to make the specimen electrically conductive. An extremely thin layer (1.5–3.0 nm) of metal, such as gold or gold palladium, is often evaporated onto the specimen in a vacuum to provide conductivity (such a thickness does not materially affect the resolution of the surface details). However, even nonconducting specimens can be analysed without the need for a metallic coating if the FESEM is operated at 1-3 kilovolts of energy. Additionally, the specimen must be able to

withstand in strong vacuum and should not cause to the change in vacuum, as by releasing gas or water molecules. Before the examining the specimen, chemically fastened nanofibrous need to be rinsed and dried to prevent damage to the fine structures caused by surface tension. In general, the metal coating on specimen is done in a separate unit.

The FE-SEM images of the investigated samples in this thesis work have been recorded by Nova Nano SEM 450 as shown in Fig. 2.9.

Figure 2.9. FESEM facilities at Central Instrument Facility (CIF) IIT (BHU).

2.3.3 Fourier Transform Infrared Spectroscopy (FTIR)

Infrared spectroscopy is an important technique for analysis of materials also gives the fingerprint of samples investigating in this work. The absorption of FTIR peaks corresponding to the frequencies of vibrations between the bonds of the atom which is responsible for building up the materials. Since no two compounds have the exact same infrared spectrum, every material has a different atom arrangement. As a result, IR spectroscopy may identify (qualitatively analyse) a variety of materials [175]. In Fig. 2.10, the Fourier transforms infrared

(FTIR) spectroscopy is depicted schematically. The FTIR is used over other infrared spectrum analyses for the reasons listed below;

- It is a non-destructive technique.
- It provides a precise measurement method which requires no external calibration.
- It can increase the speed of data collection and scan every second.
- It has greater optical throughput.
- It is mechanically simple with only one moving part.

In this thesis work, the FT-IR spectra of the powdered samples in transmission mode were recorded by an FT-IR spectrophotometer of Shimadzu; model DF 803 Japan as shown in Fig.2.10 by taking sample to KBr in 1:100 mass ratios within wavenumber range 400-4000 cm^{-1} at room temperature.

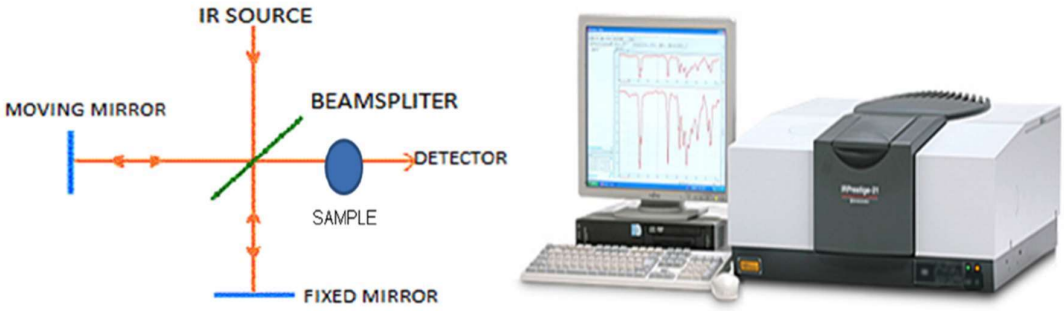

Figure 2.10. Principle of FT-IR spectroscopy and experimental set-up for FTIR measurement facility.

2.3.4 X-Ray Photoelectron Spectroscopy (XPS)

XPS is a non-destructive chemical surface analysis system that can be used to analyse the surface chemistry of materials in its as received state, or after some treatment such as; fracturing, cutting or scraping in air or UHV to explore bulk chemistry [176]. It provides the information about the presence of elements in compositions of the parts per thousand range,

empirical formula; chemical state and electronic state of the elements that exist within a material.

Photons with energies up to 10 KeV interact primarily with atomic electrons and excite it to upper energy levels (from upper core cell to vacuum level) via photon absorption process. When electrons are excited to vacuum level then this process is known as photoelectric process. This photoelectric process is a direct signature of interaction of photon with atomic electrons, forms a basis of one major analytic tool- photoelectron spectroscopy. When X-rays are used to excite atomic level electrons (primarily core level are excited) then it is known as X-ray photoelectron spectroscopy. Since core energy levels are quantized and element specific, the exited electrons have unique kinetic energy (if exited from a fixed energy source), contain signature of electronic structure of element. Normally Mo K_α or Al K_α, X- ray source is used to excite atomic level electrons and hemispherical analyzer equipped with detector is used to analyze energy spectrum of ejected photoelectrons. The ejected photoelectrons are very limited to sample surface, since the ejected electrons from the depth greater than 10nm has very less probability to eject from the sample. However, the X-rays can penetrate to higher depth. The energy of photoelectrons is well defined in the terms of binding energy of electronic level of element. If chemical environment of an atom changes it produces an energy shift in binding energy of electronic level. The energy of electron is calculated from the kinetic energy of photoelectrons, the relation is given as follows [177]:

$$\hbar\omega = E_B^F(k) + E_{kin} + \phi_{spec} \qquad (2.19)$$

where, $\hbar\omega$ is energy of photon source, $E_B^F(k)$ is binding energy of electrons, E_{kin} is kinetic energy (K.E.) of photoelectrons, ϕ_{spec} is work function of spectrometer. The energy diagram is shown in Fig. 2.11.

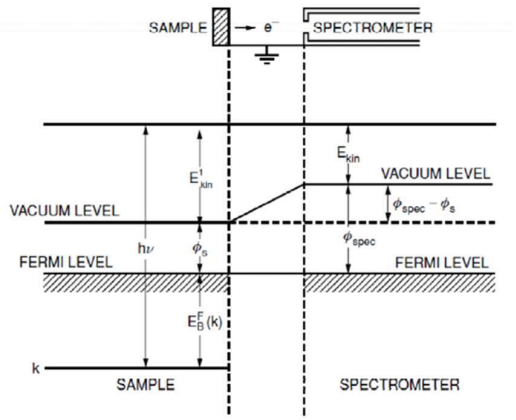

Figure 2.11. Schematic diagram of energy levels of sample and spectrometer. Note that the conducting specimen and spectrometer housing is in electrical contact [177]**.**

When photoelectron ejects from the sample, if it is insulator, then with time it may be charged if it is not properly grounded. This charging effect further reduce K.E. of photoelectrons along with in overcoming from bonding energy and work function, results in further energy shift in binding energy of ejected photoelectrons. Hence proper grounding, i.e., proper electric contact of sample with spectrometer is very important.

In general, the XPS spectra is recorded in high vacuum (P ≈ 10^{-8} milibar) or ultra-high vacuum (UHV ≈ 10^{-9} milibar) conditions, although a current area of development is an ambient pressure XPS, in which samples are analysed at various pressure of few milibar. Ion beam etching process is used to clean off the surface contamination to get more extensive and accurate analysis in-depth profiling of elements. It is also exposed in the heat to study the changes occurring by heating in chemical composition and valence states of elements. Similarly, in the exposure of reactive gases, solutions, ion beam implantation, ultra-violet light, the XPS measurement has been carried out. It is routinely used to analyze inorganic compounds, metal alloys, semiconductors, polymers, elements, catalysts, glasses, ceramics, paints, papers, inks, woods, plant parts, teeth, bones, medical implants, bio-materials, ion-modified materials, and many others. XPS is also known as ESCA (Electron Spectroscopy for

Chemical Analysis). In present thesis work, the XPS spectra of the samples have been recorded by K-Alpha, Thermo Fisher Scientific, with the pressure of 5 x 10^{-11} Torr as shown in Fig. 2.12.

Figure 2.12. XPS Facility at Central Instrument Facility (CIF) (IIT BHU).

2.3.5 Ultra-Violet Visible Near Infra-Red (UV-Vis-NIR) Spectroscopy

UV-Vis-NIR spectroscopy is an analytical technique that measures the amount of discrete wavelengths of ultra-violet, visible or near infrared that are absorbed by or transmitted through a sample in comparison to a reference or blank sample. This property is influenced by the specimen composition. In every substance or matter, a specific amount of energy is needed to promote electrons to a higher energy state which we can be sensed as absorption. Electrons in different bonding environments in a substance or matter require a different specific amount of energy to promote the electrons to a higher energy state. Since, a photon has a certain amount of energy which is inversely proportional to its wavelength. Thus, shorter wavelengths carry more energy and longer wavelengths carries less energy. This is why the absorption of photon occurs for different wavelengths in different substances. The absorption of particular wavelength carries the information about the available energy bands/levels and energy gaps.

Therefore, by analysing the absorption spectra by substances, the information of energy bands/levels and gaps can be drawn. The Jan Tauc developed a relation between absorption energy and absorbance by substance to determine the optical band gap from absorbance spectrum, known as Tauc relation. According to Tauc relation, the optical absorption strength depends on the difference between the photon energy and the band gap as follows:

$$(\alpha h\nu) = A(h\nu - E_g)^n \qquad (2.20)$$

Where, h is Planck's constant, ν is the Photon's frequency, α is absorption coefficient, E_g is the band gap and A is proportionality constant. The value of exponent n denotes the nature of the electronic transition, whether allowed or forbidden and direct or indirect: for direct allowed transition n=1/2, for direct forbidden transition n=3/2, for indirect allowed transition n=2 and for indirect forbidden transition n=3 [178]. The band gap corresponding to direct transition was obtained by extrapolating the linear portion of $(\alpha h\nu)^2$ verses hν curves such that $(\alpha h\nu)^2 = 0$.

A UV-Vis.-NIR spectrometer is used to measure the absorption of photon by specimen. In general, the UV-Vis.-NIR spectrophotometer has four main components named as (i) light source (ii) sample holder (iii) diffraction grating of monochromator (iv) detector. The radiation source is operated in continuous mode from UV-Vis.-NIR wavelengths. The photomultiplier tube, a photodiode or charge-coupled device (CCD) is used as a detector. Single photodiode detectors and photomultiplier tube are used for scanning monochromator, which filters all wavelength and pass only single wavelength to detector at one time. The scanning monochromator moves the diffraction grating to "Step-through" each wavelength so that its intensity has been measured as a function of wavelength. UV-Vis.-NIR spectrophotometer (Shimandzu, UV-2600) shown in Fig. 2.13 is used for present investigating sample.

Figure 2.13. Experimental Set-up for UV-Vis.-NIR measurement (IIT BHU).

2.3.6 Alternating Current (AC) Electrical data analysis

Figure 2.14. Experimental Set up for electrical measurements (IIT BHU).

On applying an alternating voltage or current to experimental sample, the impedance of synthesized compositions is measured using high precision LCR meter (Agilent E-4980, USA) operating between 20 Hz to 2 MHz while heating the samples at different temperatures from 30 ^{o}C to 600^{o}C. For the electrical properties measurement, the necessary electrode was

created on both the surfaces of pellets using a high temperature silver paste (Alfa Aesar). The silver coated pellets were then heated upto 500°C for 30 min to form proper electrode. The impedance of the different samples was measured in the presence of ac signal by mounting the pellet in a sample holder inside a tube furnace in an air atmosphere using two probe methods. The experimental set up used for electrical measurement for this investigation is shown in Fig. 2.14. The electrical and dielectric parameters were calculated from the measured impedance data by following relations:

$$\varepsilon_r^* = \varepsilon_r' - i\varepsilon_r'' = \frac{1}{i\omega C_0 Z^*} \qquad (2.21)$$

$$\tan\delta = \frac{\varepsilon''}{\varepsilon'} = \frac{\varepsilon_r''}{\varepsilon_r'} \qquad (2.22)$$

where, $Z^* = Z' + iZ''$ is complex impedance, ε_r' & ε_r'' are real and imaginary components of the relative permittivity ε_r^*, i is an imaginary unit ($i^2 = -1$), ω = angular frequency of the applied AC signal, $C_0 = \varepsilon_0 A/d$, ε_0 = permittivity of free space (8.85×10^{-12} Fm^{-1}), d = separation between the electrodes and A = electrode surface area.

The obtained negative dielectric constant is analysed according to Drude Lorentz (DL) model. According to the DL model, the dielectric constant is defined in Eqn. (1.18):

$$\varepsilon_r' = 1 - \frac{\omega_p^2}{\omega^2 + \gamma^2} + \frac{\omega_{pl}^2(\omega_0^2 - \omega^2)}{(\omega_0^2 - \omega^2)^2 + \omega^2\gamma^2} \qquad (1.18)$$

The electrical conductivity is calculated from the relation:

$$\sigma' + i\sigma'' = i\omega(\varepsilon_r' - i\varepsilon_r'') \qquad (2.23)$$

$$\sigma_{ac} = \sigma' = \omega\varepsilon_r''\varepsilon_0 \qquad (2.24)$$

$$\sigma'' = \omega\varepsilon_r'\varepsilon_0 \qquad (2.25)$$

$$\sigma_{ac} = \frac{\sigma_0}{1 + \omega^2\tau^2} + \frac{\varepsilon_0\omega_{pl}^2\omega^2\gamma}{(\omega_0^2 - \omega^2)^2 + \omega^2\gamma^2} \qquad (2.26)$$